

Electron Correlations in the Quasi-Two-Dimensional Organic Conductor θ -(BEDT-TTF) $_2$ I $_3$ investigated by ^{13}C NMR

Michihiro Hirata¹, Kazuya Miyagawa¹, Kazushi Kanoda¹, Masafumi Tamura²

¹ *Department of Applied Physics,
University of Tokyo, Bunkyo-ku,
Tokyo, 113-8656, Japan*

² *Department of Physics,
Faculty of Science and Technology,
Tokyo University of Science,
Noda, Chiba, 278-8510, Japan*

(Dated: February 7, 2012)

Abstract

We report a ^{13}C -NMR study on the organic conductor θ -(BEDT-TTF) $_2$ I $_3$ [BEDT-TTF: bisethylenedithio-tetrathiafulvalene] at ambient pressure. The lattice symmetry is consistent with the pseudo-orthorhombic structure by the orientation dependence of the NMR spectra, in which all molecules in the unit cell are crystallographically equivalent. There is no signature of charge disproportionation as observed in most of the θ -type BEDT-TTF salts. The analysis of NMR Knight shift, K , and the nuclear spin-lattice relaxation rate, $1/T_1$, revealed the degree of electron correlation, evaluated by the Korringa ratio ($\propto 1/T_1TK^2$), is in an intermediate regime. However, NMR relaxation rate is enhanced above 200 K, which is a possible indication that the system enters into a quantum critical regime of charge-order fluctuations as suggested theoretically.

PACS numbers:

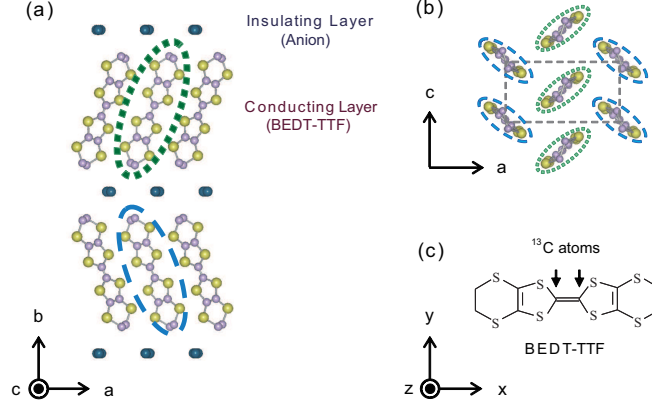


FIG. 1: (Color online) (a) Side view of the pseudo-orthorhombic crystal structure of $\theta\text{-I}_3$. (b) Top view of the schematic arrangement of BEDT-TTF molecules in the conducting ac plane. (c) Molecular principal axes of a BEDT-TTF molecule. Arrows indicate the positions of ^{13}C atoms. In figures (a) and (b), two molecules which become unequal in their geometric arrangement with respect to the field direction of $H // bc$ and $H // ac$ are represented by dotted and dashed ellipses in (a) and (b), respectively.

I. INTRODUCTION

The layered organic compounds $(\text{BEDT-TTF})_2\text{X}$ exhibit fascinating electronic phases with superconductivity¹, Mott localization², spin liquid³, charge ordering^{4,5}, massless Dirac fermions^{6,7}, and so on, where X is monovalent anion and BEDT-TTF is bisethylenedithio-tetrathiafulvalene. The system is constructed from alternate stacking of 2D conducting layers of the donor molecule BEDT-TTF and insulating layers of anion X [Fig. 1(a)]. The anion extracts an electron from two BEDT-TTF molecules, i.e., $(\text{BEDT-TTF})^{+0.5} : \text{X}^-$, which results in a quarter-filled hole band through inter-molecular overlaps of the molecular orbital.

The title compound, $\theta\text{-(BEDT-TTF)}_2\text{I}_3$ (abbreviated to $\theta\text{-I}_3$), is known as a typical 2D metal with highly symmetric zigzag alignment of BEDT-TTF molecules in the conducting layer [Fig. 1(b)]⁸. It is metallic in the whole temperature range⁸, and the Fermi surface has been confirmed by quantum oscillation^{9–14} and optical^{15,16} experiments. Magnetic susceptibility exhibits weak temperature dependence^{14,17}, characteristic of the Pauli paramagnetism. Moreover, superconductivity is observed at T_C of ca. 3.6 K^{8,18}.

Meanwhile, the isostructural materials $\theta\text{-(BEDT-TTF)}_2\text{MZn(SCN)}_4$ [$\text{M} = \text{Rb}$ and Cs]

(abbreviated to θ -MZn), undergo metal-to-insulator (MI) transitions at $T_{\text{MI}} = 195\text{K}$ (θ -RbZn) and 20K (θ -CsZn)⁴ accompanied by a spontaneous charge ordering⁵ (CO) and a glassy charge disproportionation¹⁹, respectively. Even in the conducting state above T_{MI} , where resistivity is temperature insensitive⁴, ¹³C-NMR line shows a gradual broadening^{5,19} toward T_{MI} , which is a manifestation of charge fluctuations. Thus, the electron correlation plays a decisive role in the electronic phases in θ -MZn. Despite the close similarity in the molecular arrangements between θ -MZn and θ -I₃, their contrasting ground states demonstrate a variation in the effects of electron correlations depending on the bandwidth, as pointed out by Mori *et al.*⁴.

Application of hydrostatic pressures drastically alters the electronic state in θ -I₃. Pressure dependence of the room-temperature resistivity shows a discontinuous jump at around 0.5 GPa²⁰. Under pressures above this critical value, θ -I₃ shows weak temperature dependence in resistivity²¹, a large increase in Hall coefficient²¹, and T^3 -dependence in nuclear spin-lattice relaxation rate, $1/T_1$, below 20 K²² with decreasing temperature, indicating the presence of a linearly dispersive energy band near the Fermi level^{23,24}. Notice that the same properties are also observed in α -(BEDT-TTF)₂I₃ (α -I₃) at high pressures approximately above 1.5 GPa^{6,25}, where a tilted massless Dirac cone is predicted by band-structure calculations^{7,24}. α -I₃ includes three nonequivalent molecules in the unit cell with the zigzag molecular arrangement as in the θ type²⁶. It is suggested that this α -type local site symmetry plays a significant role in the realization of the tilted Dirac cone in α -I₃^{7,27,28}. Similar argument is expected in θ -I₃ under pressure, though the crystal structure at above 0.5 GPa is not yet determined. Moreover, x-ray diffraction experiments at ambient pressure suggest two possible types of crystal structures in θ -I₃⁸, i.e., pseudo-orthorhombic lattice (space group P_{nma}) and monoclinic lattice ($P2_1/c$). This open issue should be explored from different experimental probes. In order to reveal the electronic states in θ -I₃ comprehensively, it is hence important to make a microscopic characterization of the ambient-pressure metallic state and the local site symmetry.

As seen above, θ -I₃ is a unique material to connect the physics of correlated electrons and Dirac electrons, which are both among the intensively studied issues in condensed matter physics. In the present work, we aim at elucidating the electronic properties in θ -I₃ at ambient pressure by means of ¹³C-NMR experiments for the first time. This is expected to provide a basis for understanding the conducting phase in the proximity of

CO phase and the massless Dirac fermions in organic conductors. First, we measured the orientation dependence of the ^{13}C -NMR spectra against applied field to evaluate the local-site symmetry and the hyperfine-shift tensor at the central ^{13}C sites in BEDT-TTF molecules [Fig. 1(c)]. Because the hyperfine interaction between electron and ^{13}C -nuclear spins is highly anisotropic in $(\text{BEDT-TTF})_2\text{X}$ compounds²⁹, the hyperfine-shift tensor $\delta = (\delta^{xx}, \delta^{yy}, \delta^{zz})$ at the ^{13}C sites is thereby determined, where x, y , and z represent the principal axes of the molecule [see Fig. 1(c)]. Then, we measured the Knight shift, K , and the nuclear spin-lattice relaxation rate, $1/T_1$, and determined local spin susceptibility and electron correlations in a quantitative manner, using the hyperfine-shift tensor determined. Based on the experimental data and analysis, we discuss the nature of electronic state in $\theta\text{-I}_3$ at ambient pressure.

II. EXPERIMENTAL

Single crystal of $\theta\text{-I}_3$ was prepared by the conventional electrochemical method. For the ^{13}C -NMR measurements, the central carbon sites in BEDT-TTF molecules were selectively enriched by ^{13}C atoms (nuclear spin $I = 1/2$, $\gamma_n = 10.7054$ MHz/T) with 99 % concentration [Fig. 1(c)]. All NMR measurements were performed for a single crystal at ambient pressure in a magnetic field H of approximately 6.00 T, which is rotated within the conducting ac plane and the bc plane [see Fig. 1]. NMR signals were obtained through the fast Fourier transformation of the so-called solid-echo signals, and the ^{13}C -resonance frequency of tetramethylsilane $[(\text{CH}_3)_4\text{Si}, \text{TMS}]$ was used as the origin of the NMR shift. The nuclear spin-lattice relaxation rate, $1/T_1$, was determined by the standard saturation and recovery method. The relaxation curves of nuclear magnetization were well fitted to single exponential functions over a decade.

III. RESULTS AND DISCUSSIONS

A. NMR spectra, local-site symmetry, and hyperfine-shift tensors

The local-site symmetry at the central ^{13}C positions of BEDT-TTF molecules [Fig. 1(c)] is examined by the angular profile of ^{13}C -NMR spectra, which were measured with changing (i) the angle θ between the crystal a axis and the applied field H in the ac conducting plane [Fig. 1(b)], and (ii) the angle ψ between the crystal b axis and H in the bc plane

[Fig. 1(a)]. Figures 2(a) and 2(b) show the typical angular dependence of ^{13}C -NMR spectra under H applied within ac plane (at 40 K) and under H applied within bc plane (at 100 K), respectively. Under all field orientations, the NMR spectra consist approximately of four lines at all measured temperatures. Two pairs of lines in Fig. 2(a) exhibit out-of-phase angular dependence against θ , whereas an in-phase variation is seen against ψ in Fig. 2(b).

As we mentioned in Section I, x-ray diffraction experiments suggest two types of crystal structures in θ - I_3 ; one is the pseudo-orthorhombic lattice (with space group P_{nma}) and the other is the monoclinic one (with space group $P2_1/c$) [8]. In the pseudo-orthorhombic symmetry, the unit cell contains two conducting layers and all molecules in the unit cell are crystallographically equivalent. Moreover, the inversion center locates exactly in-between the two adjacent ^{13}C atoms in a BEDT-TTF. In the monoclinic lattice, three molecules in each layer of the double-decker unit cell are crystallographically nonequivalent and only two of them have the inversion symmetry in the molecular center as in α - I_3 ³². In the ^{13}C -NMR spectra, each nonequivalent molecule gives distinct resonance lines. Furthermore, due to the nuclear dipole interaction between the adjacent ^{13}C nuclei, each resonance line from a molecule splits into a doublet or a quartet depending on whether the molecule has the inversion symmetry or not²⁷. In case of the pseudo-orthorhombic lattice, when H is applied within ac plane, the two layers in the unit cell are equivalent while the two differently oriented molecules in a layer become unequal with respect to the field H . On the contrary, when H is applied within bc plane, the two adjacent layers are unequal whereas the two differently oriented molecules in a layer become equivalent with respect to H . Thus, only two molecules with inversion centers are unequal against magnetic field H in both field geometries and four lines (two pairs of doublets) are expected for the pseudo-orthorhombic lattice. In case of the monoclinic lattice, however, three molecules (one without and two with inversion centers) are unequal in a layer against an arbitrary field direction. Thus, eight lines (one quartet and two doublets) are expected under the ac -plan-field geometry and they should be doubled under the bc -plane-field one, where the adjacent layers are unequal. It is obvious that the observed four-line structures in Figs. 2(a) and 2(b) are fully consistent with the pseudo-orthorhombic lattice. A small peak splitting in several spectra, e.g., at $\theta = 20^\circ, 30^\circ, 40^\circ, 50^\circ$, and 60° in Fig. 2(a), is attributable to a slight misalignment of the rotating plane of H from ac plane. Even if the split lines are counted as independent lines, the number of lines is much less than what is expected in the monoclinic lattice.

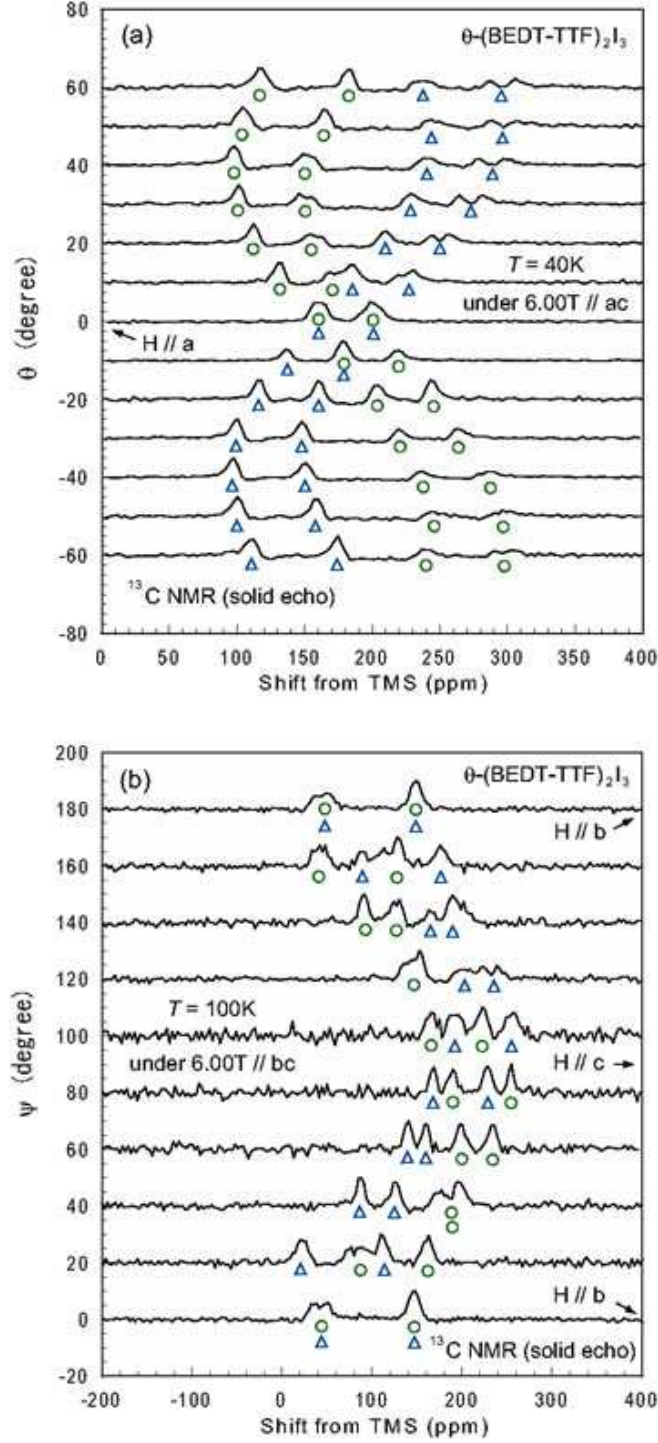


FIG. 2: (Color online) Orientation dependence of the ^{13}C -NMR spectra (a) under H within ac plane (40 K) and (b) under H within bc plane (100 K). The θ and ψ are field angles from a and b axes, respectively. Symbols represent different Pake doublets stemming from the two differently oriented molecules in the double-decker unit cell (See Fig. 1).

This becomes clearer when we look into the angular dependence of the NMR line structure in more detail. Based on the pseudo-orthorhombic symmetry, we assigned the observed four lines into two Pake doublets, as denoted by circles and triangles in Figs. 2(a) and 2(b), stemming from the two differently oriented molecules in the unit cell [dotted and dashed ellipses in Fig. 1(b) for the lines in Fig. 2(a), and those in Fig. 1(a) for the lines in Fig. 2(b)].

Figures 3(a) and 3(b) show the splitting width, d , of each doublet. The solid and dashed curves represent the calculated angular dependence of d , which is expressed as $d = (3/2r^3)\gamma_n^2\hbar(1 - 3\cos^2\theta)^{29}$, where $\gamma_n = 10.7054\text{MHz/T}$ is the gyromagnetic ratio of ^{13}C nucleus, $2\pi\hbar$ is the Planck constant, r denotes the distance between the adjacent ^{13}C nuclei, and θ is the angle between H and the molecular x axis [see Fig. 1(c)]. We used the crystal structure reported by Kobayashi *et al.*³³ and optimal $r = 0.135\text{ nm}$ ³⁴. The calculated curves are in good agreement with the observed splitting width.

Figures 4(a) and 4(b) depict the angular dependence of the ^{13}C -NMR shift given by the midpoint of each Pake doublet under $H//ac$ and $H//bc$ at 100 K, respectively (the same symbols as in Figs. 2 and 3 are used). We performed a least square fit of sinusoidal curves to these data sets in Figs. 4(a) and 4(b) simultaneously with the three principal values of the hyperfine-shift tensor as fitting parameters based on the crystal structure³³. The resulting fitting curves are shown by solid and dashed curves in Figs. 4(a) and 4(b), where the principal values of the hyperfine-shift tensor are uniquely determined as $(\delta_{xx}, \delta_{yy}, \delta_{zz}) = (67, 134, 300)$ (in ppm). Again, the agreement between the calculated curves and the experimental data are fairly well. From all these arguments, it is concluded that all of the BEDT-TTF molecules in $\theta\text{-I}_3$ are electronically equivalent, being consistent with the local symmetry of the pseudo-orthorhombic lattice. This agrees well with the quantum oscillation⁹⁻¹⁴ and optical reflectance^{15,16} experiments both of which confirmed a round and large Fermi surface predicted by the band-structure calculation with the pseudo-orthorhombic symmetry⁸. It is noted that, if the three crystallographically non-equivalent molecules in the monoclinic structure are not electronically distinctive, this case is not ruled out.

It is also noteworthy to mention that each line in the NMR spectra is much narrower ($\sim 1\text{kHz}$) in the whole temperature range than the cases in $\theta\text{-RbZn}$ and $\theta\text{-CsZn}$ which exhibit NMR line splitting or broadening over several kHz or more in association with the charge ordering and its glassy freezing, respectively^{5,19}. The present spectral feature

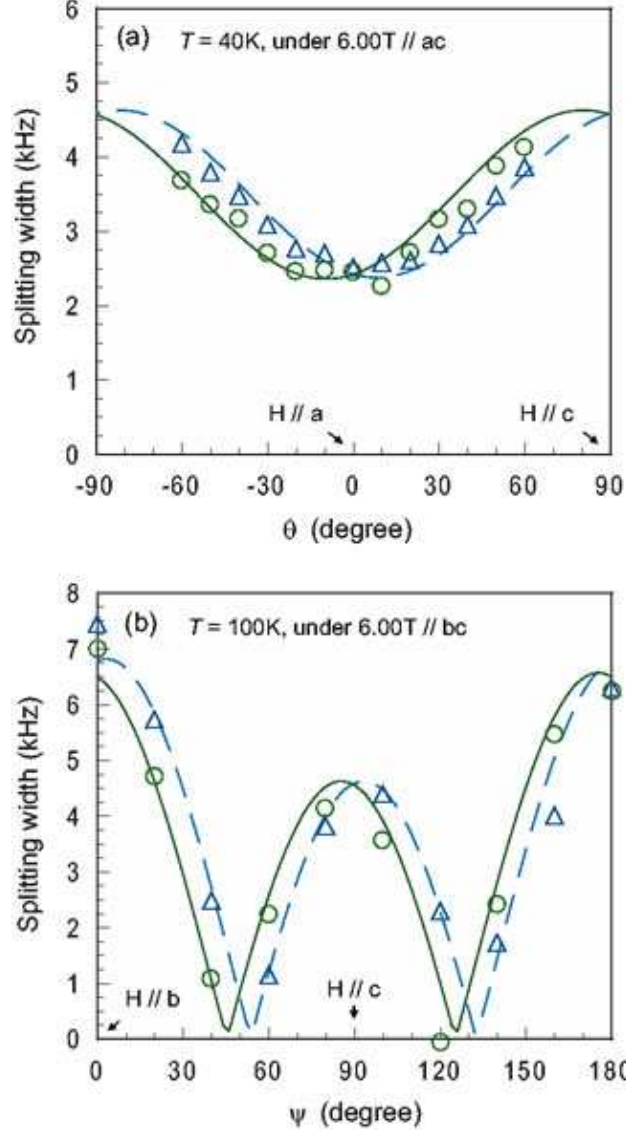


FIG. 3: (Color online) Angular dependence of the nuclear dipole splitting width d at the two differently oriented molecules in the unit cell (denoted by symbols) under (a) $H//ac$ (40K) and (b) $H//bc$ (100K), extracted from Figs. 2(a) and 2(b), respectively. The same symbols are used as in Fig. 2. Calculated angular dependence is shown by solid and dashed curves based on the crystal structure reported by Kobayashi *et al.*³³ and the optimal $^{13}\text{C}=^{13}\text{C}$ bond length of $r = 0.135 \text{ nm}$ ³⁴.

clearly indicates that $\theta\text{-I}_3$ at ambient pressure is free from these instabilities of the charge organization. This is consistent with the sharp line width observed in Raman scattering experiments³⁵.

As mentioned in Section I, the metallic phase of $\theta\text{-I}_3$ is changed at 0.5 GPa to the massless

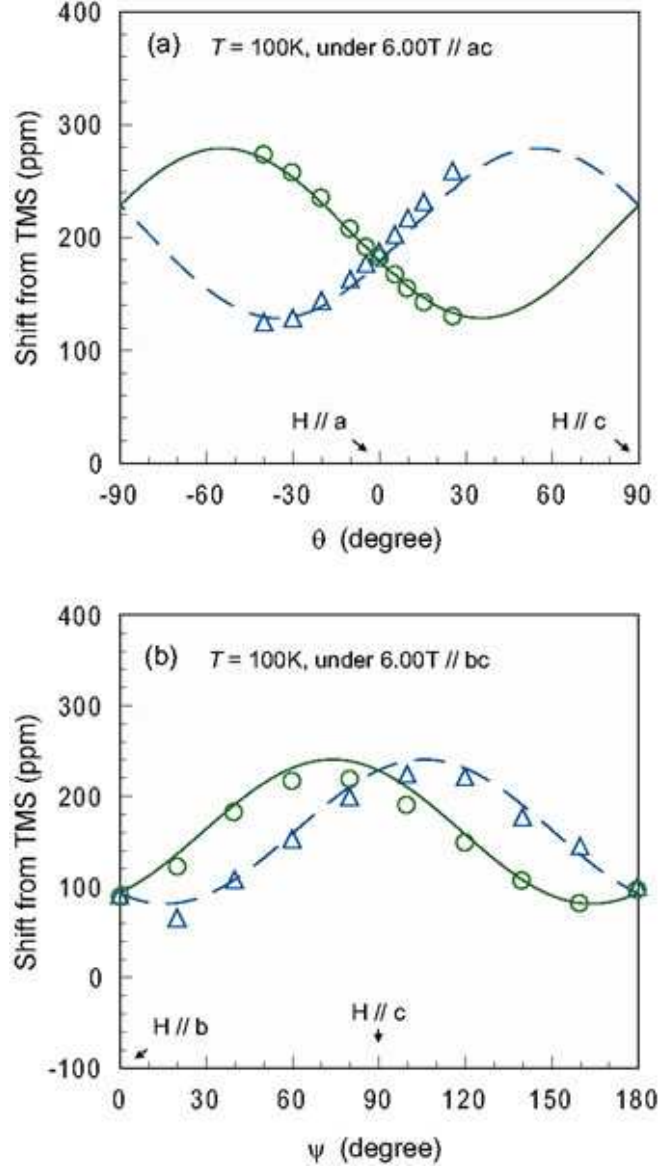


FIG. 4: (Color online) Angular dependence of the averaged ^{13}C -NMR shift d (central line shift of a Pake doublet) at the two unequal molecules in the unit cell (symbols) at (a) $H \parallel ac$ (100 K) and (b) $H \parallel bc$ (100 K). The same symbols are used as in Figs. 2 and 3. Curves stand for the least square fits to the data calculated from the crystal structure³³ and the hyperfine-shift tensor given in the text.

Dirac fermions with a linear energy-momentum dispersion, which is confirmed later by ^{13}C -NMR shift and relaxation-rate measurements performed at 0.8 GPa²². Noticeably, NMR spectra in the high-pressure phase exhibit more than eight lines. The qualitative difference in the spectral feature below and above 0.5 GPa evidences that the transition at 0.5 GPa

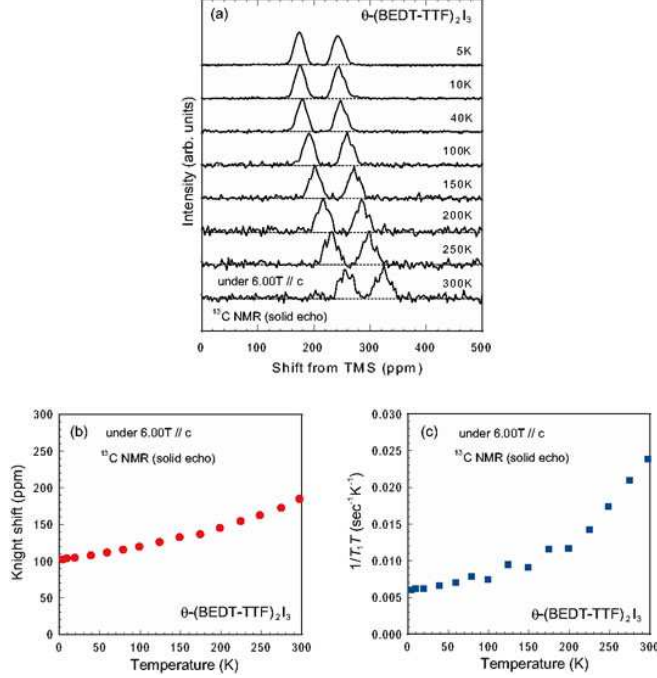


FIG. 5: (Color online) (a) Temperature dependence of the ^{13}C -NMR spectra under $H//c$ in the 2D conducting plane. (b), (c): Temperature dependence of the Knight shift, K ($= \delta - \sigma$; with the central NMR line shift δ and the temperature-independent chemical shift $\sigma \approx 106$ ppm) and the nuclear spin-lattice relaxation rate, $1/T_1$, divided by temperature T under the same field orientation ($H//c$).

accompanies a structural phase transition with a symmetry reduction; thereby $\theta\text{-I}_3$ is very probably transformed into a new structure similar to $\alpha\text{-I}_3$ that accommodates the massless Dirac fermions.

B. Knight shift, nuclear spin-lattice relaxation rate, and electron-correlation effect

Next, we turn our attentions to the local electronic structures in $\theta\text{-I}_3$ at ambient pressure. We measured the temperature dependence of ^{13}C -NMR spectra, which gives Knight shift, K , and nuclear spin-lattice relaxation rate, $1/T_1$.

Figure 5(a) shows the temperature dependence of the ^{13}C -NMR spectra under an external field H of 6.00 T applied parallel to the c axis in the conduction layer. All molecules become equivalent under this field orientation, so only a single Pake doublet is observed.

The spectra show moderate temperature dependence with decreasing temperature. The

NMR shift, δ , defined as the midpoint of the doublet, is composed of the Knight shift, K , and the chemical shift, σ , terms, i.e., $\delta = K + \sigma$. The Knight shift, K , is related to the electron spin susceptibility χ_s via $K = a\chi_s/2\mu_B N_A$, where a is the hyperfine-coupling constant, μ_B is the Bohr magneton, and N_A is Avogadro's number. The chemical shift, σ , originates from the orbital motion of electrons in a BEDT-TTF molecule and is temperature independent. In the present field configuration, it is estimated as $\sigma \approx 106$ ppm from the chemical-shift tensors reported by Kawai *et al.*^{36,37} and the pseudo-orthorhombic crystal structure³³. By subtracting σ from the NMR shift δ , we evaluated the Knight shift K ($= \delta - \sigma$) as shown in Fig. 5(b). It decreases monotonically with temperatures with a slight concave around 200 K, approaching a value of 100 ppm in the low-temperature limit. The temperature dependence of Knight shift K is more prominent than that of the spin susceptibility χ_s determined by magnetization measurements earlier¹⁴.

Figure 5(c) shows the temperature dependence of nuclear spin-lattice relaxation rate $1/T_1$ divided by temperature, $1/T_1 T$, under the same field orientation ($H//c$). $1/T_1 T$ exhibits a monotonic decrease with decreasing temperature. Compared with the Knight shift K shown in Fig. 5(b), $1/T_1 T$ shows relatively large temperature dependence, which seems to get steeper above ca. 200 K. In a metallic system, $1/T_1$ is proportional to the scattering rate of conducting electrons by nuclear spins near the Fermi level E_F and is known, in case of isotropic hyperfine interaction characterized by the coupling constant a , to follow the Korringa relation³⁸ — $1/T_1 T = 4\pi k_B/\hbar(\gamma_n/\gamma_e)^2 a^2(\mu_B/2N_A)^2 \langle D(E_F)^2 \rangle_T$ — where $D(E_F)$ is the electronic density of states at E_F , γ_e is the gyromagnetic ratio of electron, and $\langle x \rangle_T$ stands for the thermal average of the quantity x . In a conventional metal without electron-electron correlations, the following relation holds between Knight shift K and relaxation rate $1/T_1$; $(1/T_1 T)K^{-2}(\hbar/4\pi k_B)(\gamma_e/\gamma_n)^2 = 1$. In (BEDT-TTF)₂X compounds, however, the hyperfine interaction is strongly anisotropic at the ¹³C positions because of a significant contribution of dipolar interactions from the p_z orbitals. This effect introduces a geometrical form factor in the above relation, namely, $(1/T_1 T)K^{-2}(\hbar/4\pi k_B)(\gamma_e/\gamma_n)^2 = \beta(\zeta, \eta)$ ^{29,32} with

$$\beta(\zeta, \eta) = \frac{(a^{xx}/a^{zz})^2(\sin^2 \eta + \cos^2 \zeta \cos^2 \eta) + (a^{yy}/a^{zz})^2(\cos^2 \eta + \cos^2 \zeta \sin^2 \eta) + \sin^2 \zeta}{2[(a^{xx}/a^{zz}) \sin^2 \zeta \cos^2 \eta + (a^{yy}/a^{zz}) \sin^2 \zeta \sin^2 \eta + \cos^2 \zeta]^2}, \quad (1)$$

where (a^{xx}, a^{yy}, a^{zz}) are the principal values of the ¹³C-hyperfine-coupling tensor, ζ is the angle between the external field H and the z -principal axis shown in Fig. 1(c), and η is

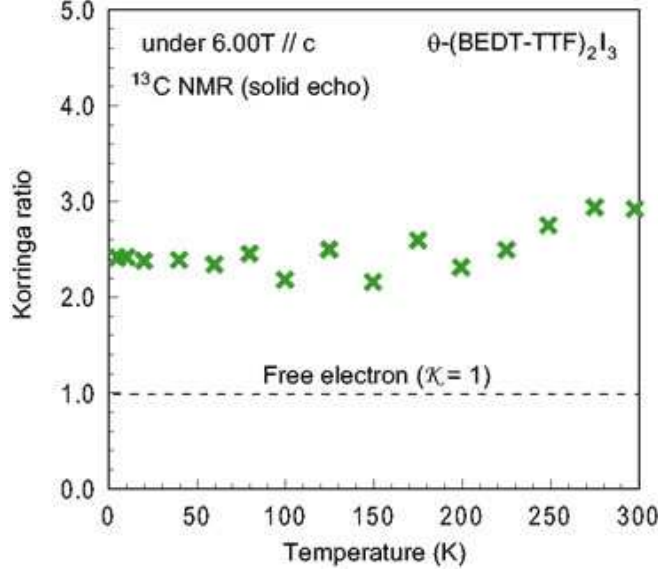


FIG. 6: (Color online) Temperature dependence of the ^{13}C -NMR Korrington ratio, $\mathcal{K} \propto (1/T_1TK^2)$, under $H//c$. The dashed line stands for the free electron's case, $\mathcal{K} = 1$ (see the text).

the polar angle measured from the x -principal axis in the xy plane of Fig. 1(c). $\beta(\zeta, \eta)$ is dependent on the orientation of the applied field H relative to the molecular axes. Furthermore, the effect of the electron correlations is incorporated into the form by the introduction of the factor, \mathcal{K} , called the Korrington ratio which measures the degree of spin fluctuations quantitatively²⁹, i.e., $(1/T_1T)K^{-2}(\hbar/4\pi k_B)(\gamma_e/\gamma_n)^2 = \beta(\zeta, \eta)\mathcal{K}$. \mathcal{K} is unity for free electrons, while it becomes larger (smaller) than unity if there are antiferromagnetic (ferromagnetic) spin fluctuations³⁹. Using the hyperfine-shift tensor determined in Section III.A, the susceptibility χ_s at 100 K reported by Salameh *et al.*¹⁴ ($\chi_s = 4.9 \times 10^{-4}$ emu/mol formula unit), and the chemical-shift tensors determined by Kawai *et al.*^{36,37}, we estimated the principal values of the ^{13}C -hyperfine-coupling tensor as $(-1.1, -0.9, 5.6)$ (in kOe/ μ_B). Then, $\beta(\zeta, \eta)$ is evaluated as ≈ 0.97 with $(\zeta, \eta) = (139^\circ, 85^\circ)$ under the current field configuration ($H//c$).

With the use of Knight shift K and $1/T_1T$ in Figs. 5(b) and 5(c), and the $\beta(\zeta, \eta)$ value determined above, the temperature dependence of the Korrington ratio \mathcal{K} is obtained as shown in Fig. 6. There is no strong temperature dependence in the Korrington ratio \mathcal{K} , which is 2.4 ± 0.2 up to 200 K and tends to increase into a value of 3.0 around room temperature. The value greater than unity points to the presence of antiferromagnetic spin fluctuations but is appreciably smaller than the typical values in strongly correlated electron systems realized in similar organic conductors. For instance, the 2D metal with strong electron

correlations, κ -(BEDT-TTF)₂Cu[N(CN)₂]Br and κ -(BEDT-TTF)₂Cu(NCS)₂^{40–42}, locating in the vicinity of Mott transition², show the Korringa ratio of $\mathcal{K} \sim 8$ at ambient pressure. The present value of \mathcal{K} hence indicates that electrons in θ -I₃ are moderately correlated. This is consistent with the experiments of quantum oscillations^{9–14} giving an effective mass which is approximately a half of the κ -type salts’.

The overall results show no signature of charge ordering unlike most of the θ -type compounds. However, it should be noted that a steep increase in $1/T_1T$ above 200 K [Fig. 5(c)] is a feature not seen in other metallic salts⁴³ and implies an enhancement of spin scatterings. The feature that the enhancement is less prominent in \mathcal{K} (Fig. 6) suggests that the spin scatterings are distributing over a wide range in the \mathbf{k} -space and are irrelevant to antiferromagnetic instabilities. Recently, Cano-Cortes and coworkers⁴⁴ theoretically investigated the extended Hubbard model with a modeled q-type structure. Among the consequences is the possible quantum phase transition of charge order with respect to the strength of electron correlations^{44,45}. In the metallic side in the phase diagram, the system is predicted to exhibit a crossover from a Fermi liquid to an incoherent bad metal with quantum critical charge fluctuations at a finite temperature T^* , which depends on the distance from the quantum critical point in the phase diagram. In the incoherent state above T^* , the spin lifetime is expected to be shortened without preferential scattering vector. The turnabout behavior in $1/T_1T$ around 200K can be a signature of this crossover. Assuming that the largest transfer integral, t_a , in θ -I₃ is 80 meV as deduced from the analysis of optical data¹⁵, 200 K corresponds to a reduced temperature of $T^*/t_a = 0.2$, which is in a reasonable range in the prediction⁴⁴. A related feature is seen in the optical conductivity measurements by Tanaka *et al.*⁴⁶ who observed a rapid loss of electronic coherence with increasing temperature. These experimental and theoretical results suggest that θ -I₃ is situated not so far away from the charge-ordering point.

IV. CONCLUSION

We performed ¹³C-NMR measurements for a single crystal of θ -(BEDT-TTF)₂I₃ at ambient pressure to probe microscopically the nature of the metallic state, which is a rare case in the θ -type family of compounds. The orientation dependence of the NMR spectra revealed that the lattice symmetry can be well understood by the pseudo-orthorhombic

symmetry with a homogeneous molecular arrangement. The NMR shift and relaxation rate $1/T_1$ measurements showed the Korringa relation up to room temperature with the weakly temperature-dependent Korringa ratio \mathcal{K} ($= 2 \sim 3$), which indicates that θ -(BEDT-TTF)₂I₃ is in a moderately correlated regime. However, the enhancement of relaxation rate, observed above 200 K, is a possible signature of the quantum critical charge fluctuations as suggested by a recent theoretical study.

V. ACKNOWLEDGEMENTS

The authors thank H. Kobayashi for informing us of the structural data before publication. This work is supported by MEXT Grant-in-Aids for Scientific Research on Innovative Area (New Frontier of Materials Science Opened by Molecular Degrees of Freedom; Grants No. 20110002 and No. 21110519), JSPS Grant-in-Aids for Scientific Research (A) (Grant No. 20244055) and (C) (Grant No. 20540346), and MEXT Global COE Program at University of Tokyo (Global Center of Excellence for the Physical Sciences Frontier; Grant No. G04).

-
- ¹ T. Ishiguro, K. Yamaji, and G. Saito, *Organic Superconductors*, Springer, Berlin (1997); A.G. Lebed, *The Physics of Organic Superconductors and Conductors*, Springer, Berlin (2008).
 - ² K. Miyagawa, K. Kanoda, and A. Kawamoto, Chem. Rev. **104**, 5635-5653 (2004); K. Kanoda and R. Kato, Annu. Rev. Condens Matter Phys. **2**, 167-88 (2011).
 - ³ Y. Shimizu, K. Miyagawa, K. Kanoda, M. Maesato, and G. Saito, Phys. Rev. Lett. **91**, 107001 (2003).
 - ⁴ H. Mori, S. Tanaka, and T. Mori, Phys. Rev. B **57**, 12023 (1998).
 - ⁵ K. Miyagawa, A. Kawamoto, and K. Kanoda, Phys. Rev. B **62**, R7679 (2000).
 - ⁶ N. Tajima, S. Sugawara, M. Tamura, Y. Nishio, and K. Kajita, J. Phys. Soc. Jpn. **75**, 051010 (2006).
 - ⁷ S. Katayama, A. Kobayashi, and Y. Suzumura, J. Phys. Soc. Jpn. **75**, 054705 (2006).
 - ⁸ H. Kobayashi, R. Kato, A. Kobayashi, Y. Nishio, K. Kajita, and W. Sasaki, Chem. Lett. **1986**, 789 (1986); H. Kobayashi, R. Kato, A. Kobayashi, Y. Nishio, K. Kajita, and W. Sasaki, Chem.

- Lett. **1986**, 833 (1986; A. Kobayashi, R. Kato, H. Kobayashi, S. Moriyama, Y. Nishio, K. Kajita, and W. Sasaki, Chem. Lett. **1986**, 2017 (1986).
- ⁹ K. Kajita, Y. Nishio, T. Takahashi, W. Sasaki, R. Kato, H. Kobayashi, and A. Kobayashi, Solid State Commun. **70**, 1181-1188 (1989).
- ¹⁰ S. J. Klepper, G. J. Athas, J. S. Brooks, M. Tokumoto, T. Kinoshita, N. Tamura, and M. Kinoshita, Synth. Metals **70**, 835-836 (1995).
- ¹¹ M. Tokumoto, A. G. Swanson, J. S. Brooks, M. Tamura, H. Tajima, and H. Kuroda, Solid State Commun. **75**, 439-444 (1990).
- ¹² M. Tamura, H. Kuroda, S. Uji, H. Aoki, M. Tokumoto, A. G. Swanson, J. S. Brooks, C. C. Agosta, and S. T. Hannahs, J. Phys. Soc. Jpn. **63**, 615-622 (1994).
- ¹³ T. Terashima, S. Uji, H. Aoki, M. Tamura, M. Kinoshita, and M. Tokumoto, Solid State Commun. **91**, 595-598 (1994).
- ¹⁴ B. Salameh, A. Nothardt, E. Balthes, W. Schmidt, D. Schweitzer, J. Strempler, B. Hinrichsen, M. Jansen, and D. K. Maude, Phys. Rev. B **75**, 054509 (2007).
- ¹⁵ M. Tamura, K. Yakushi, H. Kuroda, A. Kobayashi, R. Kato, and H. Kobayashi, J. Phys. Soc. Jpn. **57**, 3239-3247 (1988).
- ¹⁶ Y. Oshima, H. Ohta, S. Okubo, K. Koyama, M. Motokawa, M. Tamura, Y. Nishio, and K. Kajita, Synth. Metals **120**, 853-854 (2001).
- ¹⁷ H. H. Wang, B. A. Vogt, U. Geiser, M. A. Beno, K. D. Carlson, S. Kleinjan, N. Thorup, and J. M. Williams, Mol. Cryst. Liq. Cryst. **181**, 135-143 (1990).
- ¹⁸ K. Kajita, Y. Nishio, S. Moriyama, W. Sasaki, R. Kato, H. Kobayashi, and A. Kobayashi, Solid State Commun. **64**, 1279-1284 (1987).
- ¹⁹ R. Chiba, K. Hiraki, T. Takahashi, H. M. Yamamoto, and T. Nakamura, Phys. Rev. Lett. **93**, 216405 (2004).
- ²⁰ M. Tamura, M. Matsuzaki, N. Tajima, Y. Nishio, and K. Kajita, Synth. Metals **86**, 2007-2008 (1997).
- ²¹ N. Tajima, A. Tajima, M. Tamura, R. Kato, Y. Nishio, and K. Kajita, J. Phys. W France **114**, 263-267 (2004).
- ²² K. Miyagawa, M. Hirayama, M. Tamura, and K. Kanoda, J. Phys. Soc. Jpn. **79**, 063703 (2010).
- ²³ B. Dora, and F. Simon, Phys. Rev. Lett. **102**, 197602 (2009).
- ²⁴ S. Katayama, A. Kobayashi, and Y. Suzumura, Eur. Phys. J. B **67**, 139-148 (2009).

- ²⁵ M. Hirata, K. Ishikawa, K. Miyagawa, K. Kanoda, and M. Tamura, unpublished.
- ²⁶ K. Bender, I. Henning, and D. Schweitzer, *Mol. Cryst. Liq. Cryst.* **108**, 359-371 (1984).
- ²⁷ T. Mori, *J. Phys. Soc. Jpn.* **79**, 014703 (2010).
- ²⁸ K. Asano, and C. Hotta, *Phys. Rev. B* **83**, 245125 (2011).
- ²⁹ A. Kawamoto, K. Miyagawa, Y. Nakazawa, and K. Kanoda, *Phys. Rev. B* **52**, 15522 (1995).
- ³⁰ Y. Takano, K. Hiraki, Y. Takada, H. M. Yamamoto, and T. Takahashi, *J. Phys. Soc. Jpn.* **79**, 104704 (2010).
- ³¹ S. Hirose, and A. Kawamoto, *Phys. Rev. B* **82**, 115114 (2010).
- ³² M. Hirata, K. Ishikawa, K. Miyagawa, K. Kanoda, and M. Tamura, *Phys. Rev. B* **84**, 125133 (2011).
- ³³ H. Kobayashi, private communications.
- ³⁴ The $^{13}\text{C}=^{13}\text{C}$ bond length r in BEDT-TTF of θ -I₃ is estimated as ~ 0.125 nm from x-ray diffraction experiment [33], which is, however, too small to reproduce our dipolar splitting width d shown in Figs. 3(a) and 3(b). This mismatch probably stems from the different mechanisms of x-ray and NMR measurements; x-ray is sensitive to the electron density distribution in a molecule, while NMR reflects the positions of the nuclei. The x-ray results possibly underestimate the bond length, for it typically has the order of $0.131 \sim 0.134$ nm [see for example P. Guionneau *et al.*, *Synth Metals* **86**, 1973-1974 (1997)]. In the present study, we estimated the bond length as ~ 0.135 nm from the fittings to the orientation dependence of d [Figs. 3(a) and 3(b)], which falls into the typical range.
- ³⁵ R. Wojciechowski, K. Yamamoto, K. Yakushi, M. Inokuchi, and A. Kawamoto, *Phys. Rev. B* **67**, 224105 (2003).
- ³⁶ T. Kawai, and A. Kawamoto, *J. Phys. Soc. Jpn.* **78**, 074711 (2009).
- ³⁷ In Ref. 35, Kawai *et al.* determined the principal components of the chemical-shift tensors in α -I₃ at ambient pressure in the CO state (60K) for the four nonequivalent molecules (i.e., molecules A, A', B, and C). These chemical-shift tensors are basically independent on molecular arrangements and is reasonably turned over to θ -I₃. However, as the authors of Ref. 35 pointed out, the principal components are strongly dependent on the amount of charge (hole) on the molecule. In the CO state of α -I₃, the charge valence is roughly estimated as A : A' : B : C = 0.8 : 0.2 : 0.8 : 0.2 [T. Kakiuchi *et al.*, *J. Phys. Soc. Jpn.* **76**, 113702 (2007)]. On the other hand, the charge is homogeneous with 0.5 valences in θ -I₃ within the present experimental accuracy.

Therefore, we took an average of chemical-shift tensors of the four independent molecules in α -I₃, which yields $(\sigma^{xx}, \sigma^{yy}, \sigma^{zz})_{\text{average}} = (116, 175, 55)$ ppm, and used this averaged shift tensor in the analyses throughout this work.

- ³⁸ C. P. Slichter, *Principles of Magnetic Resonance*, 3rd ed. (Springer-Verlag, New York, 1989).
- ³⁹ T. Moriya, J. Phys. Soc. Jpn. **18**, 516-520 (1963).
- ⁴⁰ H. Mayaffre, P. Wzietek, C. Lenoir, D. Jerome, and P. Batail, Eur. Phys. Lett. **28**, 205-210 (1994).
- ⁴¹ S. M. De Soto, C. P. Slichter, A. M. Kini, H. H. Wang, U. Geiser, and J. M. Williams, Phys. Rev. B **52**, 10364 (1995).
- ⁴² M. Itaya, Y. Eto, A. Kawamoto, and H. Taniguchi, Phys. Rev. Lett. **102**, 227003 (2009).
- ⁴³ K. Kanoda, Hyperfine Interactions **104**, 235 (1997); Physica C **282-287**, 299 (1997); J. Phys. Soc. Jpn. **75** 051007 (2006).
- ⁴⁴ L. Cano-Cortes, J. Merino, and S. Fratini, Phys. Rev. Lett. **105** 036405 (2010).
- ⁴⁵ M. Dressel, J. Phys.:Condens. Matter **23** 293201 (2011).
- ⁴⁶ K. Takenaka, M. Tamura, N. Tajima, H. Takagi, J. Nohara, and S. Sugai, Phys. Rev. Lett. **95**, 227801 (2005).